

Where do they come from? Identification of escaped globular cluster stars

Cheng Xu^{1,2}, Baitian Tang^{1,2}, Chengyuan Li^{1,2}, José G. Fernández-Trincado³, Jing Zhong⁴,
Long Wang^{1,2}, Hao Tian^{5,6} and Yang Huang^{5,7}

¹ Department of Astronomy, School of Physics and Astronomy, Sun Yat-sen University, Zhuhai, Guangdong Province, China
e-mail: tangbt@sysu.edu.cn

² CSST Science Center for the Guangdong-Hong Kong-Macau Greater Bay Area, Zhuhai 519082, China

³ Instituto de Astronomía, Universidad Católica del Norte, Av. Angamos 0610, Antofagasta, Chile

⁴ Key Laboratory for Research in Galaxies and Cosmology, Shanghai Astronomical Observatory, Chinese Academy of Sciences, 80 Nandan Road, Shanghai 200030, China

⁵ School of Astronomy and Space Science, University of Chinese Academy of Sciences, Beijing 100049, China

⁶ Institute for Frontiers in Astronomy and Astrophysics, Beijing Normal University, Beijing, 102206, China

⁷ Key Laboratory of Space Astronomy and Technology, National Astronomical Observatories, Chinese Academy of Sciences, Beijing 100101, China

Received –, –; accepted –, –

ABSTRACT

Globular clusters (GCs), as old as our Galaxy, constantly lose their members to the field as they cross through the Milky Way (MW). These escaped GC stars (or escapees) are thought to contribute significantly to the MW halo. If a star left the host GC a long time ago, chemical finger prints (e.g., N enrichment) may reveal its origin. In this work we aim to establish dynamical connections between N-rich field stars recently identified by LAMOST and the existing MW GCs. By constructing the full action distribution in combination with metallicity, we found 29 potential GC progenitors for 15 N-rich field stars. In particular, some of them may be related to MW accretion events. On the other hand, if a star has recently left its host GC via tidal evaporation, it still maintains the kinematic properties of the cluster. Here we identify extra-tidal candidates based on their spatial locations, proper motions (PMs), and their positions on color-magnitude diagrams (CMDs). We successfully identified more than 1600 extra-tidal candidates in the vicinity of six Gaia-Enceladus (GE)-related GCs: NGC 1851, NGC 1904, NGC 6205, NGC 6341, NGC 6779, NGC 7089. The density map of the extra-tidal candidates is confirmed to be an efficient way to find extra-tidal structures. The two possible density peaks at opposite sides of the inner boundary is a good indicator for a long stellar stream. Among 95 extra-tidal candidates with spectroscopic radial velocities and metallicity, 54 of them are confirmed to be GC escaped stars as they share similar properties to host GCs. These extra-tidal candidates are ideal targets for follow-up spectroscopic observation as it greatly improves the scientific outcome. Once a statistically significant number of spectroscopic radial velocities and metallicities are available, the GC dynamical evolution (e.g., mass loss, rotation) can be carefully investigated.

Key words. globular clusters – N-rich stars – extra-tidal stars

1. Introduction

In recent years, large spectroscopic surveys, such as the Apache Point Observatory Galactic Evolution Experiment (APOGEE; [Abdurro'uf et al. 2022](#)), the Gaia-ESO survey (GES; [Randich et al. 2022](#)), the Large Sky Area Multi-Object Fibre Spectroscopic Telescope (LAMOST; [Cui et al. 2012](#); [Deng et al. 2012](#); [Zhao et al. 2012](#)), Galactic Archeology with HERME (GALAH; [Buder et al. 2021](#)), and the Radial Velocity Experiment (RAVE; [Steinmetz et al. 2020](#)), have provided radial velocities and chemistry of a large number of stars in the MW. At the same time, the Gaia space mission ([Gaia Collaboration et al. 2016](#)) has also delivered astrometry, radial velocity, and chemical information for billions or millions of stars. The combining dataset yields six-dimensional space-velocity information and multiple dimensions in chemical abundances, which not only helps us evaluate the dynamical evolution of different scale of stellar systems (e.g., star clusters, galaxies), but also promotes the development of Galactic archaeology.

With such a rich dataset and with such unprecedented detail, the MW is finally showing its true nature to us. It devoured nearby dwarf galaxies during its growth, such as the recent victim, the Sagittarius dwarf elliptical galaxy ([Ibata et al. 1994](#); [Belokurov et al. 2006](#)). There are other digested casualties, for example the Gaia-Enceladus (GE, [Helmi et al. 2018](#); [Belokurov et al. 2018](#)) and Sequoia Galaxies ([Myeong et al. 2019](#)), which are now part of the inner MW halo and thick disk. During this process, some GCs, which originally formed in dwarf galaxies, were later brought into the MW as the dwarf galaxies were accreted by the MW.

Due to the tidal evaporation and binary ejection, GC stars are continuously lost to the field ([Anguiano et al. 2015, 2016](#); [Kundu et al. 2019, 2021](#); [Fernández-Trincado et al. 2021a](#); [Solima 2020](#)). The main escape mechanism is tidal evaporation (~ 80%, [Weatherford et al. 2023](#)), where stars preferentially escape through Lagrangian 1 and Lagrangian 2 points formed by the combined potentials of GCs and the MW. As these escaped stars (or escapees) rotate differentially around the MW, stellar

streams are created (Odenkirchen et al. 2001; Grillmair & Diatonos 2006; Jordi & Grebel 2010; Kuzma et al. 2018; Malhan et al. 2018; Ibata et al. 2019; Wan et al. 2020). Stellar streams do not persist forever as they eventually disperse to become part of the MW. These GC escapees are the key to answering questions related to MW-GC coevolution, for example determining the percentage of GC escapees in the MW halo and the initial mass distribution for GCs, understanding how galaxy accretion affects GC evolution, and whether these escapees also show signatures of dense star clusters, for example multiple populations (MPs; see below).

Tracing these escapees in the enormous number of MW stars is not an easy task, the astronomical community started the identification only recently using kinematic and chemical properties, thanks to the rich survey data. As tidal evaporation is the main escape mechanism, we should expect that the escapees around GCs share similar kinematic properties with their host GCs. For example, using the data from Gaia DR2 (Gaia Collaboration et al. 2018) and SDSS DR14 (Abolfathi et al. 2018), Hanke et al. (2020) established associations between 151 extra-tidal stars in the neighborhood of eight GCs by estimating the dynamical likelihood between modeled stellar streams and extra-tidal stars. Following this, by utilizing the Gaia EDR3 (Gaia Collaboration et al. 2021), Kundu et al. (2021, 2022) obtained proper motions (PMs) and constructed color-magnitude diagrams (CMDs) to search within $1-5r_t$ of multiple GCs, leading to the identification of numerous extra-tidal candidates. While some of these candidates exhibited tidal tails near specific GC (e.g., NGC 2808), the majority of extra-tidal candidates showed no significant external structures in the GC's vicinity.

On the other hand, the chemical signatures of GCs can also help the identification of GC escapees, as chemistry is more stable than kinematics. The distinct chemical signature of GCs is known as multiple populations (Carretta et al. 2010; Mészáros et al. 2015; Milone et al. 2015b; Mészáros et al. 2015; Bastian & Lardo 2018; Tang et al. 2017, 2018, 2021; Li et al. 2021). This phenomenon refers to the variations in light element abundances in GC members. Traditionally, GC stars with enhanced N and Na (and sometimes He and Al) and reduced C and O (and sometimes Mg) are called the second population (2P), while the primordial population is called 1P. It is generally accepted that such chemical anomalies are formed mostly in dense environments, such as GCs (Gratton et al. 2012; Bastian & Lardo 2018). So searching for 2P-like stars is a feasible way to find the association between GC escapees and the ejecting and/or dissolving GCs. Nitrogen is an obvious targeted element as it is connected to many molecular lines in the optical and near-infrared (NIR), such as NH or CN molecules, making its abundance easier to obtain. A large number of N-rich field stars have been discovered through high-resolution spectral surveys (see, e.g., Lind et al. 2015; Martell et al. 2016; Majewski et al. 2017; Schiavon et al. 2017; Fernández-Trincado et al. 2016, 2017, 2019b,a, 2020a,b,c,d, 2021b, 2022). Alternately, low-resolution spectra observations can expand the search to fainter and larger sample of stars (Martell & Grebel 2010; Martell et al. 2011; Koch et al. 2019). In this quest, LAMOST DR5 offered ~ 100 newly identified N-rich metal-poor field stars Tang et al. (2019, 2020). A larger sample size of N-rich field stars increases the credibility of the drawn statistical results.

There are still debated questions related to GC escapees, for example, whether it is possible to find the host GC for a given N-rich field star so that we can trace each escaped incident throughout the galaxy evolution or if we can find escapees in the vicinity of GCs with similar kinematic properties so that we can estimate

the star loss. We try to address these two questions in this work. This is also part of our recently proposed project “Scrutinizing GALaxy-STaR cluster coevolutiON with cheomOdynaMIcs (GASTRONOMI),” which investigates the interplay between the MW, nearby satellite dwarf galaxies, and star clusters using photometric and spectroscopic data. This project bridges star evolution and galaxy evolution with solid foundations, which may also help us understand exotic objects in the early universe.

This paper is structured as follows. We first describe the methodology (Section 2), and then we present and discuss the possible associations between escaped N-rich field stars and their host GCs (Section 3.1). We found extra-tidal candidates of six GE GCs using PM and CMDs, and we carefully discuss them case by case, for example checking metallicities ($[Fe/H]$) and RVs of the extra-tidal star candidates to confirm their origin (Section 3.2). Finally, we summarize our results and give suggestions for further studies (Section 4).

2. Methods

2.1. Method I: Integrals of motion

To identify the host GC for a given N-rich field star, we calculate their integral of motion (IoM), and find if they match in this parameter space. There are two assumptions here. First, the MW potential is axisymmetric and steady-state because orbits in such a potential have a conservative IoM (Binney & Tremaine 2008). The second assumption is that N-rich field stars escaped GCs with evaporation, so that they share similar kinematic properties. The latter assumption is true for $\sim 80\%$ of escapees, according to Weatherford et al. (2023).

2.1.1. Data

In this work we try to establish the connection between host GC and N-rich field stars from Tang et al. (2019, 2020). In order to simulate their orbits and find their IoMs, we need to first compile a catalog of kinematic information of existing GCs and N-rich field star sample. Metallicity is also used to constrain their consistency. The N-rich field stars are metal-poor red giants with metallicity ($[Fe/H]$) in the range $[-1.8, -1.0]$ and effective temperature (T_{eff}) in the range $[4000K, 5500K]$. We retrieved their stellar parameters and radial velocity (RV) values from Tang et al. (2020), while their sky positions and PMs come from Gaia EDR3 (Gaia Collaboration et al. 2021). We used the Bayesian spectrophotometric distances with no assumptions about the underlying populations (Carlin et al. 2015) presented in Tang et al. (2020).

Next, we retrieved PMs, distances, radial velocities, and the associated uncertainties of 158 GCs from Vasiliev & Baumgardt (2021) and Baumgardt & Vasiliev (2021). We obtained their metallicity from Harris (1996) (2010 version), but there are still a few GCs (13) without literature metallicity values. As a result, a total of 145 GCs possess complete 6D kinematic parameters along with metallicity information.

2.1.2. Orbital model

We integrated orbits and computed IoMs for the stars and for the clusters using a Python package for galactic dynamics: GALPY (Bovy 2015). We adopted a steady-state and axisymmetric MW potential: MWPotential2014. The Galactic coordinates of the Sun are $(8.27, 0, 0)$ kpc. The circular velocity at the solar radius is $V_C(R_0) = 220 \text{ km}\cdot\text{s}^{-1}$ and the peculiar velocity of the Sun

is [11.1, 12.24, 7.25] km·s⁻¹ (Schönrich et al. 2010). Alternative choices of circular velocity and solar peculiar velocities are also tested (e.g., Huang et al. 2015, 2016; Zhou et al. 2023), and the results hold very well. To calculate the orbital energy E , the vertical component of the angular momentum L_z , the radial actions J_r , and the vertical actions J_z , we used the Stäckel fudge approximation in GALPY (Binney 2012). We set the backward integration time to 5 Gyr, with a time step of 5 Myr.

To estimate the uncertainties of the actions for each object (N-rich field star and GC), we ran GALPY with random kinematic parameters drawn from Gaussian distributions (expected values equal to values presented above, and standard deviations equal to their uncertainties). Given that PMRA and PMDEC measured by Gaia are correlated, their Gaussian distributions are also correlated. Then we acquired the Gaussian-liked distributions of actions for each object, which were used for the following comparison.

To establish the connection between N-rich field stars and GCs, we assumed they are consistent in actions. In addition, stars escaped from GCs should also share the same metallicity ([Fe/H]) with the GC progenitor. As done in Savino & Posti (2019), we set the metallicity uncertainties to 0.3 dex for individual stars, which is reasonable for measurements obtained from low-resolution spectra. Finally, we calculated the matching probability of each pair of N-rich field stars and GCs, with 4D Gaussian-like distributions $(J_r, J_z, L_z, [Fe/H])^T$ (also see Hanke et al. 2020). During this process, the correlations between actions are also taken into account.

2.2. Method II: Stars in globular cluster's vicinity

If a star is evaporated out of a GC, and does not leave its vicinity, the kinematic properties of this star should be consistent with the host GC. The stable stellar chemical evolution also provides another constraint in its magnitude and color. Here we try to identify escaped stars in the vicinity of six GE-related GCs with PM and CMD, which should be similar to their host GCs. We pick GCs related to GE dwarf galaxies first because some of the N-rich field stars may originate from GE (Yu et al. 2021) and second because these GCs are brought inside our MW during the accretion, which may experience stronger tidal evaporation, and thus more escaped stars. The six GCs are NGC 1851, NGC 1904, NGC 6205, NGC 6341, NGC 6779, NGC 7089, which are thought to be related to GE, according to Massari et al. (2019), Limberg et al. (2022) and Malhan et al. (2022). The basic parameters of these six GCs are shown in Table 1.

2.2.1. Data quality selection

To identify escaped stars by PM and CMD with high confidence, we retrieved high-quality astrometric and photometric data from Gaia EDR3. We adopted the following selection criteria recommended by Gaia (Gaia Collaboration et al. 2016, 2021):

- (1) $RUWE < 1.4$
RUWE is the re-normalized unit weight error. A small value means a good fit by a single star model.
- (2) $ASTROMETRIC_EXCESS_NOISE_SIG < 2$
Excess noise refers to the extra noise in each observation that causes the residual scatter in the astrometric solution. If $ASTROMETRIC_EXCESS_NOISE_SIG$ is greater than two, then this excess noise cannot be ignored.
- (3) $ASTROMETRIC_GOF_AL < 3$

This parameter represents the goodness of fit between the astrometric model and the observed data. A high value indicates a poor fit.

- (4) $VISIBILITY_PERIODS_USED > 10$
This parameter represents the number of visibility periods used in the astrometric solution. A high number of visibility periods is a better indicator of an astrometrically well-observed source.¹
- (5) $0.001+0.039(BP-RP) < \log_{10} excess_flux < 0.12+0.039(BP-RP)$
This parameter primarily constrains whether the sources have consistent fluxes. The sources that are outside of this range may be extended sources.
- (6) $Plx < 0.5$
Due to the large distance of the selected GCs, it becomes very difficult to estimate the distance via the Gaia parallax. However, we can exclude foreground stars with large parallax ($Plx > 0.5$).

For each GC, we applied these criteria to stars within five times the King tidal radius (r_t). The escaped stars are defined to satisfy these criteria: 1) in the range $1-5r_t$; 2) having similar PM to stars inside $1 r_t$; 3) on the same CMD outlined by stars inside $1 r_t$. Such stars are traditionally called “extra-tidal candidates” in the literature. We show the r_t and the Jacobi radius (r_J) of six GCs in Table 1. The stars beyond the r_J are completely out of the gravitational potential of the cluster. However, the stars that are between the r_t and the r_J may be loosely bound to the cluster (see, e.g., Fukushige & Heggie 2000; Baumgardt et al. 2010; Küpper et al. 2010).

2.2.2. PM selection

Before identifying extra-tidal candidates via PM, we need to estimate the PM distribution of stars inside r_t . Here we utilized the Python package **Scikit-Learn** (Pedregosa et al. 2011) to build a Gaussian mixture model (GMM) with two different distributions, one for the cluster stars with a smaller dispersion in PM and another for field stars with a larger dispersion. We set up a full covariance to account for asymmetric distribution. We obtained the mean, standard deviation, and correlation coefficient of the two best-fitting Gaussian distributions, representing the average PM and corresponding dispersion of cluster stars and field stars, respectively.

The best-fitting results are shown in Fig. 1, with mean PM and dispersion listed in Table 1. Among our investigated GCs, the mean PMs of the cluster stars are consistent with the observed cluster PMs from Baumgardt & Vasiliev (2021) (red stars). We also tested multiple-Gaussian models, for example with three or four components (Kundu et al. 2022), but we did not find a significant difference compared to the case with two components.

We found that the PM distribution of cluster stars was not a simple symmetric distribution, indicating that PMs in RA and DEC are correlated. Therefore, we could not simply adopt the observed cluster PM and its dispersion. Instead, we needed to estimate the PM distribution of the cluster stars, and extrapolate to the surrounding area of the cluster (within $1-5r_t$). To this end, we estimated their probabilities with the method and formulas presented in Section 4 of Sariya & Yadav (2015). In their formulas the mean and dispersion of PMs for both cluster and field stars were obtained from the averages and standard deviations calculated by GMM. The correlation between the two

¹ <https://gea.esac.esa.int/archive/documentation/GEDR3/>

Table 1. Kinematic parameters of six GCs studied in this work.

Name	RA [deg]	DEC [deg]	r_t^a [']	r_J^b [']	$\mu_{\alpha\cos\delta}$ [mas yr ⁻¹]	μ_{δ} [mas yr ⁻¹]	$\sigma_{\mu_{\alpha}}$ [mas yr ⁻¹]	$\sigma_{\mu_{\delta}}$ [mas yr ⁻¹]	ρ
NGC 1851	78.528	-40.047	6.52	36.56	2.13	-0.62	0.38	0.46	-0.04
NGC 1904	81.046	-24.524	8.02	17.26	2.47	-1.59	0.37	0.50	0.02
NGC 6205	250.422	36.460	21.01	62.2	-3.12	-2.54	0.32	0.4	0.17
NGC 6341	259.281	43.136	12.44	48.88	-4.93	-0.66	0.4	0.42	0.18
NGC 6779	289.148	30.183	10.55	31.93	-2	1.63	0.38	0.39	-0.01
NGC 7089	323.363	-0.823	12.45	32.78	3.58	-2.19	0.6	0.38	-0.11

Notes. *a*: Harris (1996), 2010 edition; *b*: Vasiliev & Baumgardt (2021); Baumgardt & Vasiliev (2021); ρ : Correlation between two components of PM.

Table 2. Parameters of the GC used to generate the isochrones and ZAHBs.

Name	Age ¹ [Gyr]	[Fe/H] ² [dex]	Distance ³ [Kpc]	[α /Fe]	E(B-V) ² [mag]	Initial Mass on HB (IMHB) [M _⊙]
NGC 1851	9.98 ± 0.5	-1.18	11.95	0.1	0.02	0.8
NGC 1904	11.14 ± 0.5	-1.6	13.08	0.2	0.01	0.7
NGC 6205	11.65 ± 0.5	-1.53	7.42	0.3	0.02	0.7
NGC 6341	13.18 ± 0.5	-2.31	8.5	0.3	0.02	0.9
NGC 6779	13.7 ± 0.5	-1.98	10.43	0.2	0.26	0.75
NGC 7089	11.78 ± 0.5	-1.65	11.69	0.2	0.06	0.7

Notes. 1: Forbes & Bridges (2010); 2: Harris (1996), 2010 edition; 3: Baumgardt & Vasiliev (2021). The [α /Fe] and IMHB are obtained by fitting the model. The model requires [α /Fe] in the range 0-0.3 and IMHB in the range 0.7-0.9.

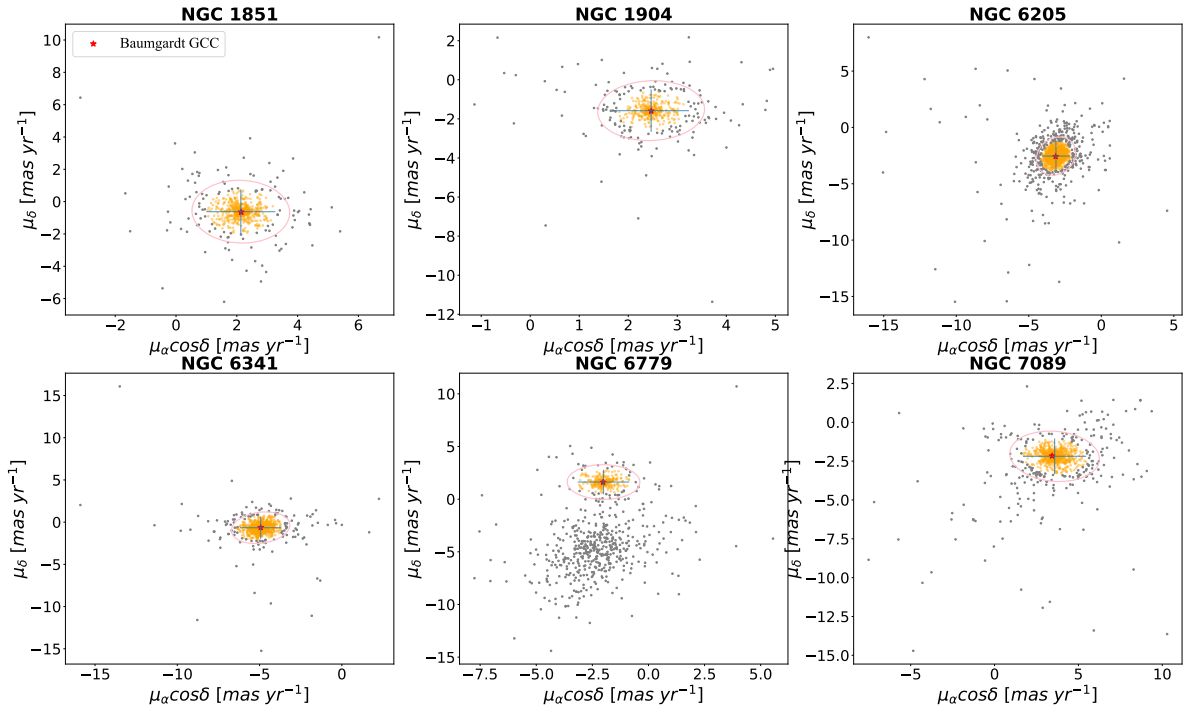


Fig. 1. PM distribution with its $\pm 3\sigma$ regions (blue lines, including 99.7% of the sample stars) of each cluster, determined as the GMM fit of the cluster stars within $1 r_t$ (orange dot), as well as the field population (gray dots). The red star in each panel represents the mean PM of clusters obtained by Baumgardt & Vasiliev (2021).

PM components was also determined by the cluster stars. This method may identify high-probability extra-tidal candidates, although with a potential drawback of underestimating their true sample size (Kundu et al. 2022).

We applied this method to six clusters and obtained a batch of extra-tidal candidates (based on PMs) for each one. Finally, for further analysis we only kept stars whose probability of having PMs compatible with the cluster PM is greater than 80%.

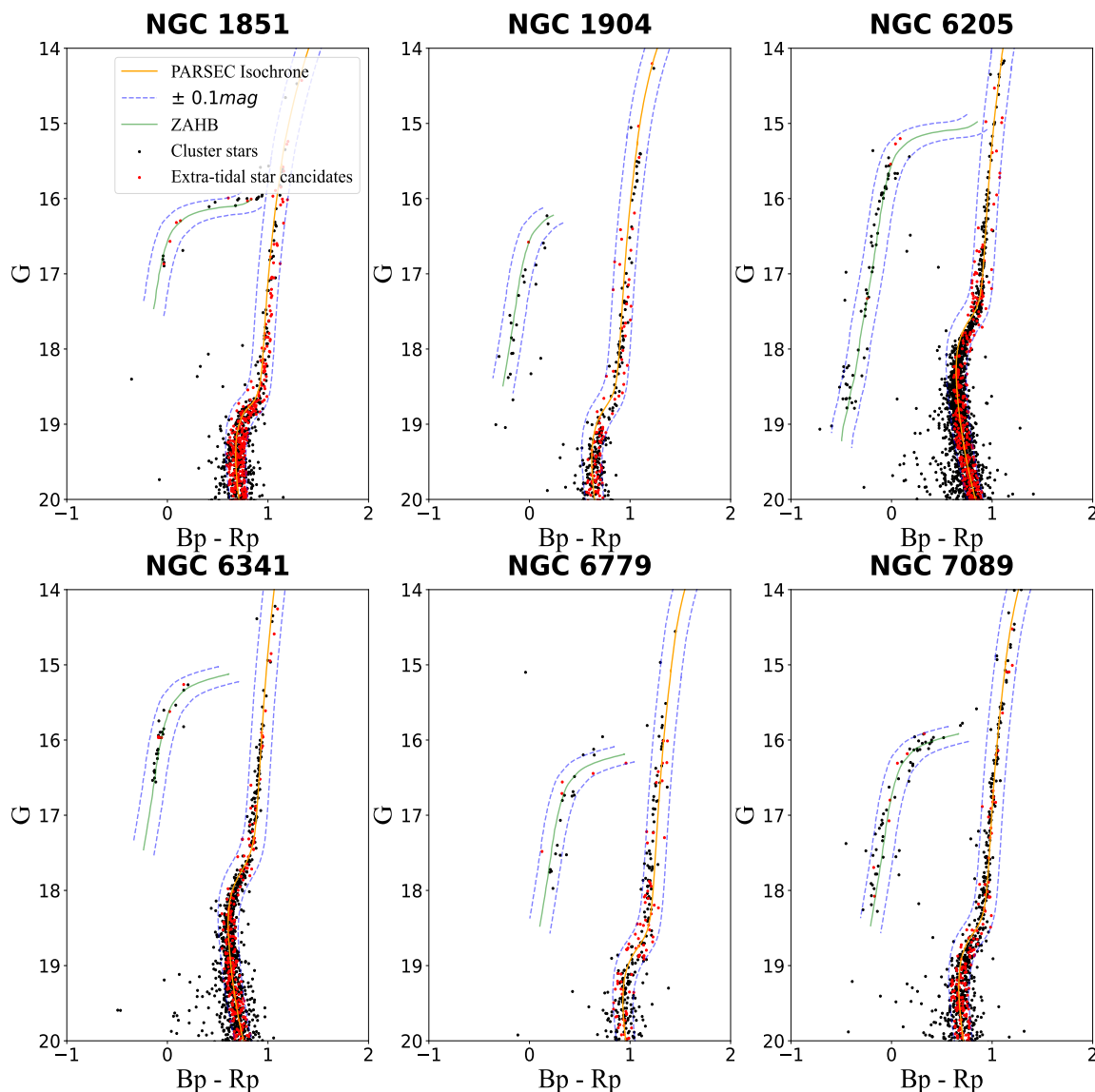


Fig. 2. Gaia EDR3 de-reddened CMD of the six GCs, with the PARSEC isochrones (solid orange lines). The ZAHB is drawn with green lines (see text for details), the red dots are the selected extra-tidal candidates, the black dots are the stars inside $1r_t$, and the blue dashed line is the boundary for selecting extra-tidal candidates.

2.2.3. Color-magnitude diagram selection

After obtaining preliminary samples by building the GMM in the PM space, we further eliminated outliers through their CMD. To construct the CMD we used Gaia EDR3 photometry. In this work we use isochrones to define outliers. We complement reddened PARSEC isochrones (Bressan et al. 2012; Marigo et al. 2017) with horizontal branch models from Valcarce et al. (2012). The model requires $[\alpha/\text{Fe}]$ in the range 0-0.3 and IMHB^2 in the range 0.7-0.9. We sampled IMHB values at intervals of 0.05 between

0.7 and 0.9, and $[\alpha/\text{Fe}]$ values at intervals of 0.05 between 0 and 0.3. Based on $[\text{Fe}/\text{H}]$ and each set of $[\alpha/\text{Fe}]$, we calculate the corresponding metallicity Z and input it into the model to generate a stellar evolutionary track. We then choose the track with the best-fitting results and record the parameters. We collected the basic parameters ($[\text{Fe}/\text{H}]$, age, distance, $[\alpha/\text{Fe}]$, IMHB) of six GCs from literature, and list them in Table 2.

In order to minimize the contamination of foreground stars, we imposed constraints on parallax. Since all six clusters in this work are located at relatively distant positions (> 5 kpc), where the parallax provided by Gaia has a relatively large uncertainty.

² Initial mass on HB

We ultimately limited the parallax to be less than $0.5''$ ($D > 2$ kpc) in order to exclude foreground stars with larger parallax values.

Figure 2 displays the cluster CMDs, PARSEC isochrones (orange lines), and zero age horizontal branch plots (ZAHB, yellow lines). Cluster stars (i.e., within $1r_t$) with PMs that match the cluster’s PM (black points) are plotted to verify the robustness of isochrones and tracks. We defined regions of ± 0.1 mag around isochrones and tracks (blue lines) to select extra-tidal candidates (red dots). Due to observational errors, fainter stars with $G > 20$ mag were excluded.

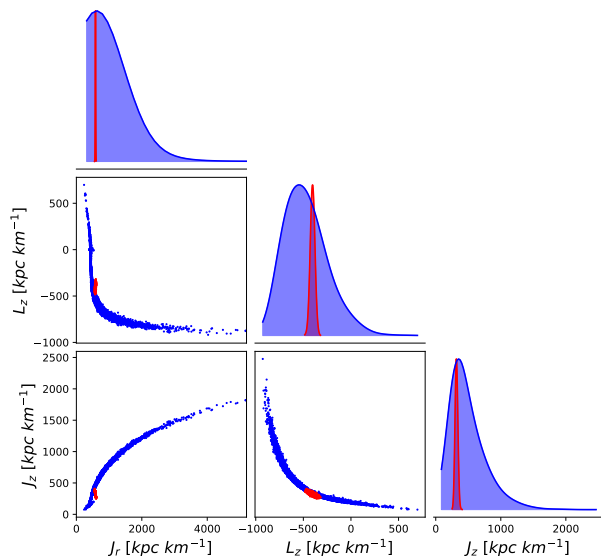


Fig. 3. Monte Carlo sample distribution of the motion integral of NGC 6779 (red) and star Gaia EDR3 1189399628220805760. The metallicity difference and p of this pair are 0.27 and 0.87, respectively. The marginal two-dimensional and one-dimensional kernel density estimates are represented by the frame and top histogram, respectively. The histograms are normalized to their maximum values for ease of presentation.

3. Results and discussion

3.1. Associating N-rich field stars with globular clusters

In this work we used IoMs to investigate the chemical and dynamical connections between N-rich field stars found in Tang et al. (2020) and existing GCs. Similar studies were recently conducted by Savino & Posti (2019) and Hanke et al. (2020), where CN-strong field stars identified from SDSS were explored. We note that the chemically peculiar stars in these three studies are all identified using the CN and CH molecular lines around 4000 \AA . These “CN-strong stars” here are called “CN-strong, CH-normal stars” to avoid confusion with other CN-strong stars caused by carbon enhancement. Furthermore, we observed a substantial portion of stars in Tang et al. (2020) with high-resolution spectra, and they are confirmed to be N-rich (Yu et al. 2021, Tang et al. in prep.).

We compared the action distributions of N-rich field stars and GCs to search for possible associations. Significant overlap may be found in individual action distribution, as shown in Fig.

3, but the overlap may be trivial in multidimensional distribution. Therefore, we use a probability (p) that considers the full distribution of actions in this work. To calculate this probability, we established a four-dimensional ($J_r, J_z, L_z, [Fe/H]$) probability density function, $\psi(\mathbf{v})$, of the different vector \mathbf{v} , for each pair of N-rich stars and GCs (Hanke et al. 2020):

$$p = \int_{\psi(\mathbf{v}') < \psi(\mathbf{0})} \psi(\mathbf{v}') d\mathbf{v}'. \quad (1)$$

We obtained matching probability (p) for 14,500 pairs of N-rich field stars and GCs. Figure 4 shows the distribution of p values versus metallicity. We categorized the results into three groups, where 1σ corresponds to $p > 0.32$, indicating that N-rich stars are closely associated with the four-dimensional distribution of the star cluster. The $1-2\sigma$ range, with p values between 0.05 and 0.32, suggests a potential association that cannot be entirely ruled out. Ultimately, we exclusively considered pairs within the 1σ range as the most likely associated pairs. We note that a p value close to 1 does not necessarily mean that the N-rich field star escaped from the corresponding GC, but rather that we cannot simply rule out the possibility of their association. Since significant kinematic errors (such as PM, radial velocity, and especially distance) can greatly affect the reliability of the results in orbit integration. In such cases, the association between the star and the GC will be determined almost solely by the distribution of metallicity. Therefore, we adopted the full distribution of actions rather than marginalized distributions for each component.

We found 137 pairs with p values greater than 0.05, of which 29 pairs had p values greater than 0.32. Among these 29 pairs, only 16 pairs had metallicities consistent within 0.3 dex. We show all results with p greater than 0.32 in Table 3. Interestingly, the majority of GCs in these pairs (17 out of 29 pairs) might be associated with accretion events (e.g., Gaia-Enceladus, Sagittarius dwarf, Helmi Streams, and Sequoia galaxy). These pairs are labeled by the last column of Table 3. This is consistent with the speculation that the MW accretion event may stimulate the escape: GC members in dissolved dwarf galaxies receive a large amount of kinematic energy from the MW during the accretion (Sparke & Gallagher 2000), leading to a higher possibility of leaving the cluster. However, precise chemical abundances are required to establish a firm connection between each star–GC pair.

A significant portion of the N-rich field stars do not seem to be chemodynamically associated with any known GC, which was also seen in the works of Savino & Posti (2019) and Hanke et al. (2020). We found that nearly 58% of N-rich stars could not be connected with any existing GC, which is slightly higher than the ratio reported by (Hanke et al. 2020, 38%) and comparable to the ratio reported by (Savino & Posti 2019, 50%). This might be due to more accurate distance measurements in this work, where smaller uncertainties lead to a less allowable tolerance for errors, and thus lower matching probabilities. Under the hypothesis that GCs are the only birth scenario for these chemically peculiar stars, these authors suggest the following reasons: 1) these stars may have escaped from GCs that have completely dissolved; 2) these stars may actually come from one of the known existing GCs, but do not retain the cluster’s orbital signature. Possible explanations for the latter scenario include high ejection velocities involving three-body interactions and early escape from the host GC, but the dramatic changes in Galactic potential energy render the steady-state potential assumption invalid.

Table 3. N-rich stars and potential GC origin from Method I. The columns list the Gaia EDR3 star ID and cluster name, the confidence measured from full action distribution combining the metallicity, and the merger events. Entries in bold are the five most probable associations

Gaia EDR3 ID	GC	Confidence (p)	m.e. ¹
4565255983145857920	NGC 5139	0.41	GE/Seq
4553384792324044928	NGC 5897	0.44	GE
4553384792324044928	NGC 6355	0.42	...
4553384792324044928	NGC 6652	0.35	...
4553384792324044928	NGC 6809	0.58	...
4526616017814192768	NGC 6544	0.38	...
4457311841406602752	NGC 5946	0.36	...
4457311841406602752	NGC 6284	0.40	GE
4452741961844020992	NGC 6712	0.56	...
3903971791408436352	NGC 2419	0.37	Sag
3903971791408436352	NGC 5272	0.48	H99
3903971791408436352	Pal 5	0.43	H99?
3903971791408436352	NGC 6235	0.34	GE
3903971791408436352	NGC 6715	0.82	Sag
3903971791408436352	Ter 8	0.50	Sag
3628877246314114176	Pal 11	0.44	...
3628603811516372864	NGC 6235	0.61	GE
2485902851604869504	NGC 4147	0.57	GE
2105942793032574592	NGC 6352	0.36	...
2095506851436919296	NGC 6121	0.52	...
1542187382923726848	NGC 5139	0.40	GE/Seq
1314804426927128960	NGC 6121	0.46	...
1189399628220805760	NGC 288	0.48	GE
1189399628220805760	NGC 6325	0.38	...
1189399628220805760	NGC 6779	0.87	G-E
915304504835769216	NGC 5904	0.45	GE/H99
915304504835769216	NGC 6584	0.70	...
912107709138952192	NGC 2419	0.39	Sag
912107709138952192	Ter 8	0.74	Sag

Notes. 1: Merger events (m.e.) that might be associated with the host GCs (Massari et al. 2019). GE stands for Gaia-Enceladus (Helmi et al. 2018); Sag stands for Sagittarius dwarf (Ibata et al. 1994); H99 stands for Helmi Streams (Helmi et al. 1999); Seq stands for Sequoia galaxy (Myeong et al. 2019).

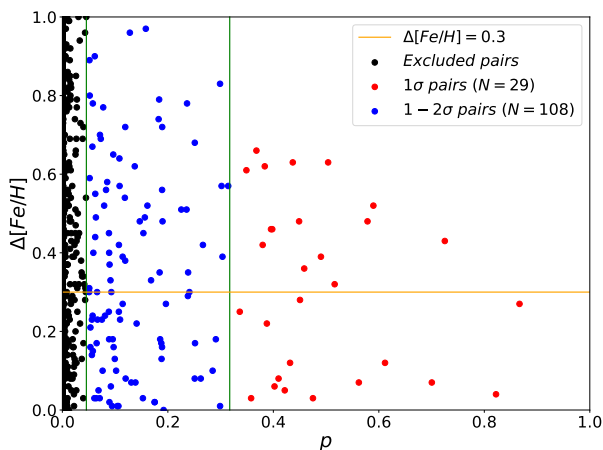


Fig. 4. For each GC–star pair, confidence level p for the pair against absolute difference in metallicity. The green lines indicate the 0.05 (1σ) and 0.32 (2σ) confidence levels. The yellow line represents an absolute difference in metallicity of 0.3. The blue dots represent pairs with a confidence between 0.05 and 0.32, while the orange dots represent pairs with a confidence greater than 0.32. The most probable pair is represented by the red dots in the bottom right region.

3.2. Extra-tidal candidates around clusters

Under the assumption of similar kinematic properties between the host GC and escaped stars in its vicinity, we explored extra-tidal candidates for six GE-related GCs. Following the selection method described in Section 2.2, we found 444, 165, 427, 286, 115, and 216 extra-tidal candidates in the vicinity of NGC 1851, NGC 1904, NGC 6205, NGC 6341, NGC 6779, and NGC 7089, respectively. The majority of these extra-tidal candidates are RGB stars or MS stars. HB extra-tidal candidates are rare: NGC 1851 (7 stars), NGC 1904 (1 star), NGC 6205 (4 stars), NGC 6341 (5 stars), NGC 6779 (5 stars), and NGC 7089 (7 stars). To investigate the possible extra-tidal features around GCs, we constructed a density map of the identified candidates (see Fig. 5). Two density peaks (i.e., NGC 1851) located in the opposite directions of the inner boundary are a strong sign of stellar streams: stars were preferentially lost from these two points, and formed stellar streams due to differential Galactic rotation.

To further confirm if these extra-tidal candidates share similar RVs and metallicities with their host GCs, we cross-matched the candidates with large spectroscopic surveys. Only a small number of stars were observed by APOGEE DR17 (Abdurro'uf et al. 2022) and SEGUE DR12 (Yanny et al. 2009; Eisenstein et al. 2011), and they are located in the vicinity of four GCs (NGC 1851, NGC 6205, NGC 6341, and NGC 7089). We define

an RV match if there is an overlap between the uncertainty range of the extra-tidal candidate and the cluster mean $RV \pm$ dispersion. A metallicity match is defined similarly. In this section the cluster's RV and dispersion are provided by [Baumgardt & Hilker \(2018\)](#);³ the cluster's mean metallicity is listed in Table 2, with an uncertainty of 0.3 dex.

3.2.1. NGC 1851

NGC 1851 is an old (9.98 Gyr, [Forbes & Bridges 2010](#)) mildly metal-poor (-1.18 dex, [Harris 2010](#)) GC located at a distance of about 11.95 kpc ([Baumgardt & Vasiliev 2021](#)). NGC 1851 is thought to have an extended halo structure that is continuously expanding ([Olszewski et al. 2009](#); [Kuzma et al. 2018](#); [Carballo-Bello et al. 2014, 2018](#)). With deep photometric data from the Dark Energy Survey (DES) and Gaia, [Shipp et al. \(2018\)](#) and [Ibata et al. \(2021\)](#) identified diffuse and long ($\sim 8^\circ$) tidal tails around NGC 1851.

In this work we found 444 extra-tidal candidate stars near NGC 1851, as shown in Fig. 6. Using high-precision PMs and CMDs from Gaia EDR3, we removed foreground stars and greatly expanded the sample of extra-tidal candidates. All stars are located within r_J , indicating that these stars are loosely bound to the cluster. Due to the high stellar density near the tidal radius of NGC 1851, we slightly expanded the inner boundary range to investigate whether NGC 1851 exhibits extended structures or stellar streams. The density distribution of the candidates (Fig. 5) appears to have two high-density peaks (> 3 Poisson noise) in the opposite direction (east–west direction), which indicates that mass loss preferentially happened in these two points. Due to the differential Galactic rotation, the GC escapees would form long stellar streams, similar to what was found in [Shipp et al. \(2018\)](#) and [Ibata et al. \(2021\)](#).

To further verify their association with NGC 1851, we looked for the detection of their RVs and metallicities. Seven stars were observed by APOGEE, and their RVs all lie within the range of cluster mean $RV \pm$ dispersion. Among them, five stars show metallicities consistent with that of the cluster, while one star does not have metallicity measurement, which does not exclude its membership. We note that extra-tidal candidates of NGC 1851 have been explored by several studies (e.g., [Marino et al. 2014](#); [Ibata et al. 2021](#)), but no common star is found between these studies and our five extra-tidal stars, mostly due to spatial difference.

3.2.2. NGC 1904

NGC 1904 is an old (11.16 Gyr, [Forbes & Bridges 2010](#)) intermediately metal-poor (-1.6 dex, [Harris 2010](#)) halo GC ($D \approx 13.08$ Kpc, [Baumgardt & Vasiliev 2021](#)). In the last few years, [de Boer et al. \(2019\)](#) have shown that the radial density distribution of this cluster can be described by an extended model within the Jacobi radius. However, deep DES photometry presented by [Shipp et al. \(2018\)](#) suggested the possible presence of a tidal tail around NGC 1904, oriented approximately north-south and extending to a radius of 1.5° . It was later confirmed by [Sollima \(2020\)](#) with Gaia DR2 data.

In this study we found 165 extra-tidal candidates around NGC 1904. Among them, 85 stars are outside r_J , which means these stars are totally unbound from the NGC 1904 (Fig. 7). Unfortunately, we found no spectroscopic observations for these stars in APOGEE, SEGUE, and LAMOST.

We then constructed density maps of extra-tidal candidates to check the extended structure of NGC 1904. We found clear density peaks along the N-S direction in the vicinity of NGC 1904 (Fig. 5), with a density exceeding three times the Poisson noise level, suggesting that NGC 1904 might have experienced significant stellar loss in these two directions (possibly L1 and L2 points). Similarly, this is a strong sign of stellar streams, which were reported by [Shipp et al. \(2018\)](#) and [Sollima \(2020\)](#).

3.2.3. NGC 6205

NGC 6205 is an old (11.65 Gyr, [Forbes & Bridges 2010](#)) intermediately metal-poor (-1.53 dex, [Harris 2010](#)) GC, with multiple population detections (e.g., [Snedden et al. 2004](#); [Johnson & Pilachowski 2012](#)). In this work we identified a total of 427 extra-tidal candidates, of which 210 are located outside of r_J . In the density map of extra-tidal candidates, we found multiple peaks (> 2), but with density values comparable to the Poisson noise level, indicating that stars might have escaped this GC more homogeneously. The possible explanations include high contamination from field stars and GC roation, but the lack of two significant peaks indicates that the tidal stream may not be easily formed, which is consistent with the conclusions drawn from the analysis of [Jordi & Grebel \(2010\)](#) and [Sollima \(2020\)](#).

Among our extra-tidal candidates, 29 stars were observed by the SEGUE survey. We identified 13 stars with RVs and metallicity consistent with those of the cluster.⁴

[Hanke et al. \(2020\)](#) identified 32 extra-tidal candidates, with 13 located within $1.2r_t$ and 19 beyond $1.6r_t$. The latter are classified as extra-tidal stars in their work. This may be due to the high stellar density near the r_t . Among our 29 extra-tidal candidates, five stars overlap with Hanke's extra-tidal sample. Only three stars⁵ show RVs and [Fe/H] consistent with the cluster under our stricter selection criteria.

3.2.4. NGC 6341

NGC 6341, one of the most metal-poor GCs (-2.31 dex, [Harris 2010](#)) in the MW, was found to have an extended outer halo ([Testa et al. 2000](#); [Jordi & Grebel 2010](#)). Recently, deep photometric observation revealed a long tidal tail (spanning $\sim 17^\circ$ on the sky) around this cluster ([Ibata et al. 2021](#); [Sollima 2020](#); [Thomas et al. 2020](#)). [Hanke et al. \(2020\)](#) identified 26 extra-tidal candidates, of which 12 were located between 12.5 and $75.2 r_t$, greatly expanding the previously assumed range of tidal debris. These authors concluded that NGC 6341 might have experienced a strong tidal field, leaving highly dispersed extra-tidal stars after tidal disruption. In this work we found a total of 286 extra-tidal candidates, of which 53 are located beyond r_J . These stars are also highly dispersed in their spatial location. In the density map (Fig. 5) we found one significant density peak (> 2 Poisson noise) along the stellar stream track toward the northwest of NGC 6341. A much weaker density peak is also found in the opposite direction, indicating that a stellar stream could have formed ([Ibata et al. 2021](#); [Sollima 2020](#); [Thomas et al. 2020](#)).

After cross-referencing with the spectral survey, we found a total of 48 stars with SEGUE observations among our candidates, of which 13 lacked metallicity information. Among the remaining 35 stars, we compared their RV distribution and [Fe/H],

⁴ Stars with significantly different RVs and [Fe/H] are not shown here due to the limited dynamical range.

⁵ GAIA EDR3 ID 1328125006003407360, 1328123601557429888, 1328116244270330368

³ <https://people.smp.uq.edu.au/HolgerBaumgardt/globular/>

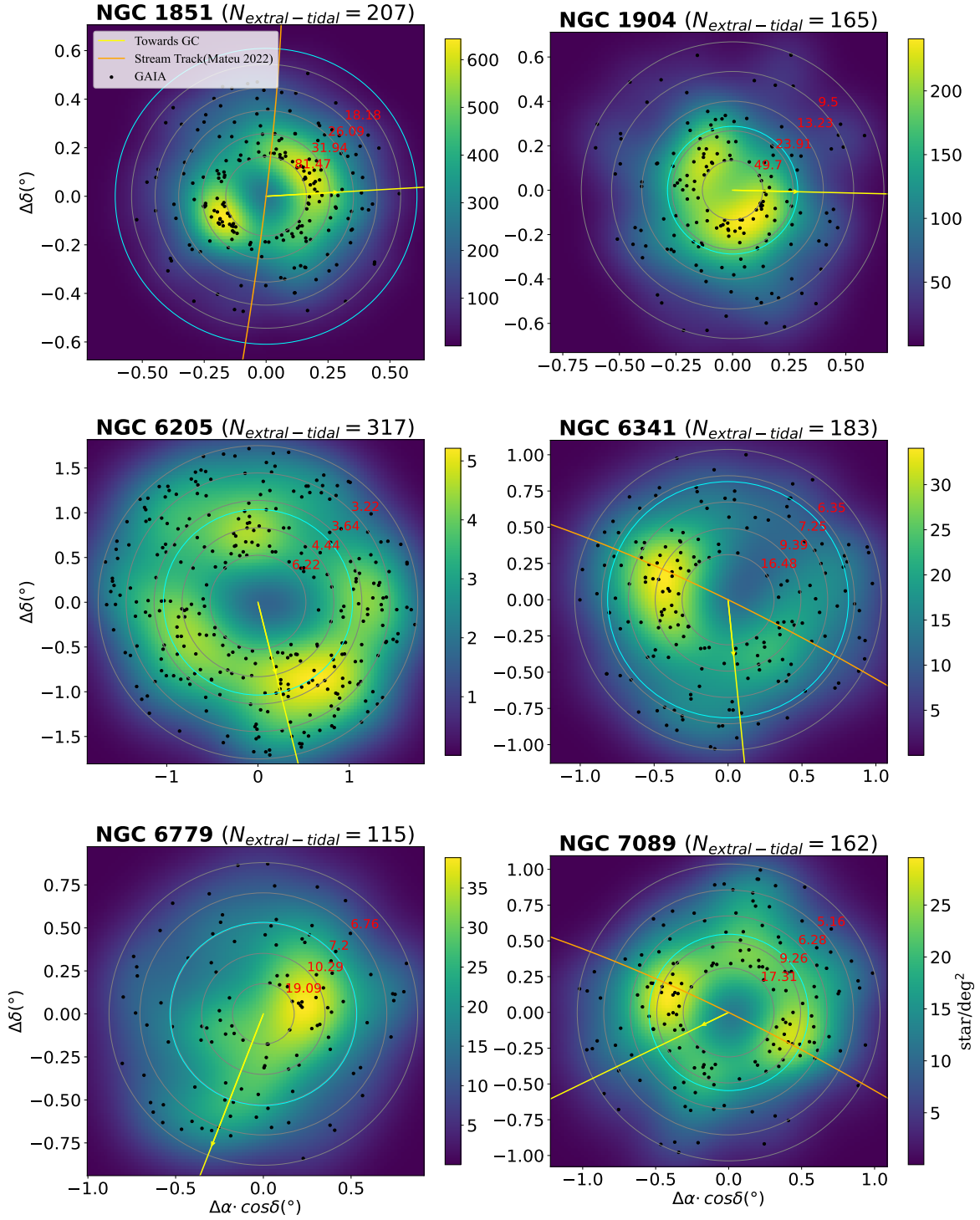


Fig. 5. Density map of extra-tidal candidates for six GCs. The spatial density of extra-tidal candidates (black dots) are indicated by their colors. The yellow line represents the direction pointing toward the Galactic center, while the orange line represents the stream track provided by [Mateu \(2023\)](#) with a parallel shift to make sure that the track goes through the cluster center. The gray circles represent the selected range, where the innermost gray circle represents the tidal radius, the outermost gray circle represents five times the tidal radius, and the blue circle represents the Jacobi radius. The average radial Poisson noise is calculated in four regions, and the values are indicated by the red text.

Table 4. Identified extra-tidal stars from Method II.

Gaia EDR3 ID	GC	RV	[Fe/H]	Spectral source	Gaia EDR3 ID	GC	RV	[Fe/H]	Spectral source
		[km·s ⁻¹]	dex				[km·s ⁻¹]	dex	
4819295189806128512	NGC 1851	318.21	-1.10	APOGEE DR17	1360418074825605888	NGC 6341	-124.24	NaN	SEGUE DR12
4819281785211829248	NGC 1851	317.53	-1.44	APOGEE DR17	1360395706636272384	NGC 6341	-131.71	NaN	SEGUE DR12
4819292681545239552	NGC 1851	323.27	-1.17	APOGEE DR17	1360192198202792960	NGC 6341	-117.86	-2.10	SEGUE DR12
4819195546567853440	NGC 1851	319.64	-1.15	APOGEE DR17	1360457352307630080	NGC 6341	-124.80	-2.04	SEGUE DR12
4819202040557645568	NGC 1851	321.22	-0.96	APOGEE DR17	1360197970638757120	NGC 6341	-118.26	-2.55	SEGUE DR12
1328127243689705728	NGC 6205	-245.26	-1.59	SEGUE DR12	1360224668155504896	NGC 6341	-114.24	-2.41	SEGUE DR12
1331385646389205632	NGC 6205	-239.46	-1.68	SEGUE DR12	1360206968594956032	NGC 6341	-113.24	-2.39	SEGUE DR12
1328116244270330368	NGC 6205	-234.83	-1.58	SEGUE DR12	1360219720353705344	NGC 6341	-116.13	-2.19	SEGUE DR12
1328118718171299328	NGC 6205	-241.40	-1.70	SEGUE DR12	1360211508375698688	NGC 6341	-122.29	-2.34	SEGUE DR12
1328123391094186752	NGC 6205	-249.97	-1.63	SEGUE DR12	1360413023944914816	NGC 6341	-121.24	-1.99	SEGUE DR12
1328126002435827840	NGC 6205	-246.05	-1.56	SEGUE DR12	1360186009153430144	NGC 6341	-122.56	-1.99	SEGUE DR12
1328125006003407360	NGC 6205	-252.85	-1.82	SEGUE DR12	1354437216903606144	NGC 6341	-117.40	-2.29	SEGUE DR12
1327315426141900672	NGC 6205	-245.22	-1.51	SEGUE DR12	1360201505396486016	NGC 6341	-133.85	-2.21	SEGUE DR12
1328071954566404736	NGC 6205	-255.31	-1.67	SEGUE DR12	1360211577095721088	NGC 6341	-120.55	-2.23	SEGUE DR12
1331385646389205632	NGC 6205	-248.86	-1.65	SEGUE DR12	1360417215833016576	NGC 6341	-122.24	-2.43	SEGUE DR12
1328063437654350976	NGC 6205	-252.65	-1.50	SEGUE DR12	1360381898322080384	NGC 6341	-126.08	-2.46	SEGUE DR12
1328123601557429888	NGC 6205	-247.03	-1.60	SEGUE DR12	1360401208495084288	NGC 6341	-121.80	-2.15	SEGUE DR12
1328136688314520960	NGC 6205	-236.12	-1.38	SEGUE DR12	1354372758034296576	NGC 6341	-119.76	-2.58	SEGUE DR12
1360144021554095744	NGC 6341	-129.98	NaN	SEGUE DR12	2686871720073157504	NGC 7089	-3.85	NaN	SEGUE DR12
1360396222033324032	NGC 6341	-133.22	NaN	SEGUE DR12	2686795819414993792	NGC 7089	-5.97	NaN	SEGUE DR12
1360191781589539072	NGC 6341	-144.51	NaN	SEGUE DR12	2686857254624358656	NGC 7089	8.13	NaN	SEGUE DR12
1360427420676038144	NGC 6341	-139.68	NaN	SEGUE DR12	2686927211051932032	NGC 7089	3.38	-1.66	SEGUE DR12
1360399898525361024	NGC 6341	-127.29	NaN	SEGUE DR12	2686854437125995648	NGC 7089	10.42	-1.51	SEGUE DR12
1360212603591009664	NGC 6341	-105.03	NaN	SEGUE DR12	2686833237167039232	NGC 7089	12.15	-1.50	SEGUE DR12
1360412061872257920	NGC 6341	-111.33	NaN	SEGUE DR12	2686896806981288704	NGC 7089	6.04	-1.36	SEGUE DR12
1360454118192779776	NGC 6341	-102.27	NaN	SEGUE DR12	2686893710305935616	NGC 7089	-6.79	-1.67	SEGUE DR12
1360454358710919040	NGC 6341	-123.53	NaN	SEGUE DR12	2686632065193630848	NGC 7089	-9.44	-1.42	SEGUE DR12

Notes. A list of all confirmed extra-tidal stars. NaN indicates no metallicity determination.

and ultimately identified 16 stars that are consistent with the cluster distribution, including 7 stars with two observations that both meet the cluster RV and [Fe/H] requirement. In addition, 7 of the 35 candidates overlapped with Hanke’s results, of which 6 were retained as extra-tidal stars, and 1 star⁶ was excluded due to a large difference in metallicity (-1.6 dex) compared to the cluster (-2.31 dex). For the 13 extra-tidal candidates with only RV observations, we also examined their RV distribution. We include them in left bottom panel of Fig. 9 where 11 stars fall within the expected range of the cluster’s RV. We will consider them to be extra-tidal stars until subsequent metallicity measurements are available.

3.2.5. NGC 6779

NGC 6779 is an extremely old (13.7 Gyr, Forbes & Bridges 2010), metal-poor (-1.98 dex, Harris 2010) GC ($D \approx 10.43$ Kpc, Baumgardt & Vasiliev 2021). Recently, Piatti & Carballo-Bello (2019) constructed the radial distribution map of the outer regions of the cluster using horizontal branch and main sequence stars and found that NGC 6779 may have an extended halo structure. However, due to the limited depth of the observations, the data did not cover the fainter main sequence stars, and there has been no clear observational evidence in recent years to confirm the extended structure.

Our work identified 115 extra-tidal candidates, of which 58 are located beyond the r_f , as shown in Fig. 7. Due to the low number density of extra-tidal candidates, no reliable structure was found in its density map (Fig. 5).

3.2.6. NGC 7089

NGC 7089 is an old (11.78 Gyr, Forbes & Bridges 2010) intermediately metal-poor (-1.65 dex, Harris 2010) halo GC ($D \approx 11.65$ Kpc, Baumgardt & Vasiliev 2021), which shows multiple stellar populations (e.g., Piotto et al. 2012; Milone et al. 2015a;

⁶ Gaia EDR3 ID 1360223598707925376

Yong et al. 2014). There are possible detections of extra-tidal structures associated with this GC: Kuzma et al. (2016) found evidence of a power-law envelope, Ibata et al. (2021) and Grillmair (2022) discovered a long tidal tail. We have identified a total of 216 extra-tidal candidates, of which 87 are located outside of r_f , as shown in Fig. 11. In the density distribution of extra-tidal candidates (Fig. 5), we discovered two density peaks along the east–west direction (with an upward trend toward the northwest by $\sim 10^\circ$). Although this density peak is weaker (~ 2 Poisson noise) compared to NGC 1851 and NGC 1904, it still indicates the presence of a stellar stream structure. This alignment is in good agreement with the direction of the stellar stream structure described in Ibata et al. (2021). Although their analysis of the NGC 7089 stellar stream structure was based on a limited number of data points, and our investigated extra-tidal region of NGC 7089 was also limited, both results indicate the potential presence of a stellar stream near NGC 7089. To confirm the existence or determine the length of the stellar stream for NGC 7089, deep photometry and RV will be required to identify additional stream member stars.

Out of the 216 candidates that we identified, 11 have SEGUE observation. By comparing the RVs and [Fe/H] of these stars with the individual RV distribution of NGC 7089, we identified six stars that are consistent with the cluster. Among these 11 candidates, 2 stars⁷ were previously identified in Hanke et al. (2020), which were also identified by this work as extra-tidal stars. Similar to NGC 6341, for the five extra-tidal candidates with only RV observations, three stars are identified as extra-tidal stars, which are also plotted in the bottom left panel of Fig. 11.

In total, we confirmed 54 extra-tidal stars around six GE-related GCs out of 95 stars with spectroscopic information (Table 4). Except for Hanke et al. (2020), we do not find overlap with other literature studies to our best knowledge. According to our experiments of extra-tidal candidates with spectroscopic ob-

⁷ GAIA EDR3 ID: 2686896806981288704, 2686893710305935616

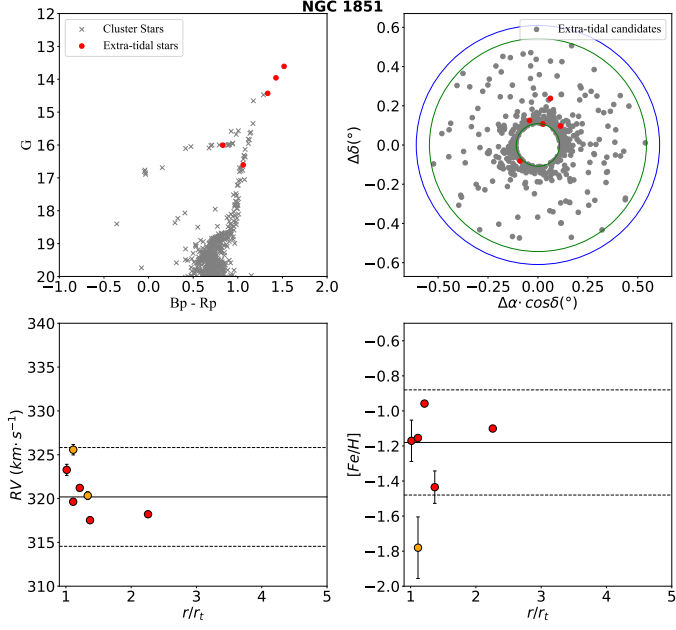


Fig. 6. CMD, spatial distribution, radial velocity, and metallicity distribution of the cluster and extra-tidal candidates based on Gaia EDR3 photometry (Gaia Collaboration et al. 2021). The gray crosses in the upper left panel represents cluster stars that are located within $1 r_t$ and whose star PM matches that of the GC. The gray points in the upper right panel represent the extra-tidal candidates selected following the method described in Section 2.2. The red points represent extra-tidal candidates with RV and $[Fe/H]$ compatible with the cluster. The green circles represent 1 and 5 tidal radii, and the blue circle represents the Jacobi radius. In the bottom two panels the orange points represent stars with radial velocity and metallicity observations that do not match the cluster. The solid horizontal line represents the mean value of the cluster, and the dashed horizontal line represents the corresponding dispersion or error range for cluster. The error bar represents the observation error of the individual stars.

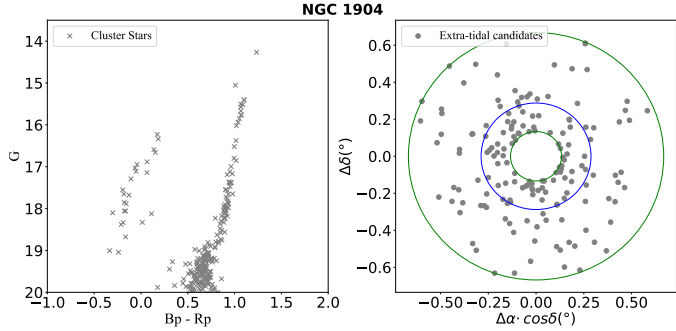


Fig. 7. Same as Fig. 6, but only CMD and spatial distribution for NGC 1904.

servations, the successful rate of selecting extra-tidal candidates that have RVs and metallicities consistent with clusters is high ($\sim 57\%$). This is a necessary step for target selection in spectroscopic surveys (e.g., SDSS, LAMOST, 4MOST) in order to maximize the scientific outcome. With RVs from a large sample of extra-tidal candidates, it is promising to construct the dynamical environment of GCs, and even their rotation (Wan et al. 2021).

In these six GE-related GCs, we found that stellar streams may be related to their extra-tidal structures and orbits. The density map of extra-tidal candidates that we identified with PMs

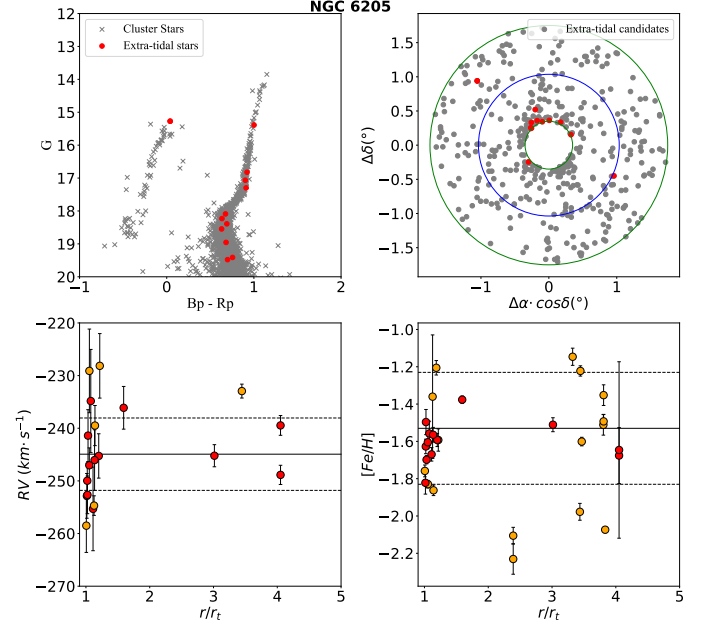


Fig. 8. Same as Fig. 6, but for NGC 6205.

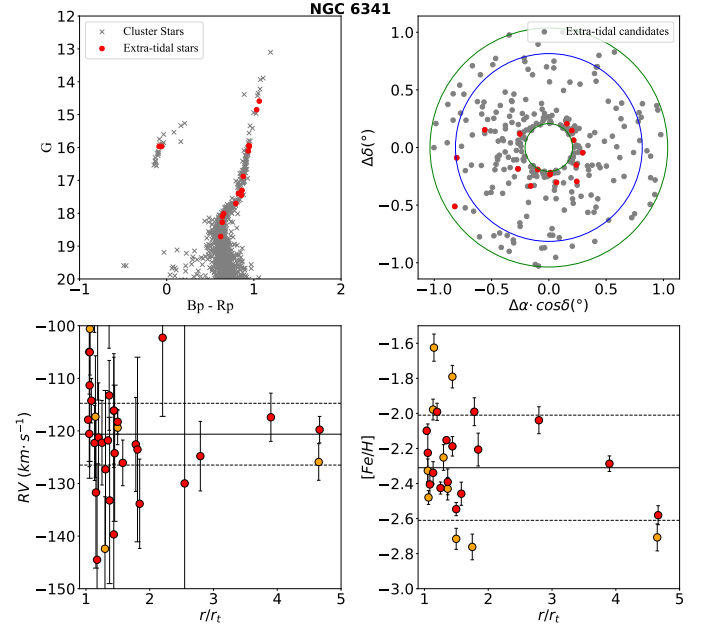


Fig. 9. Same as Fig. 6, but for NGC 6341.

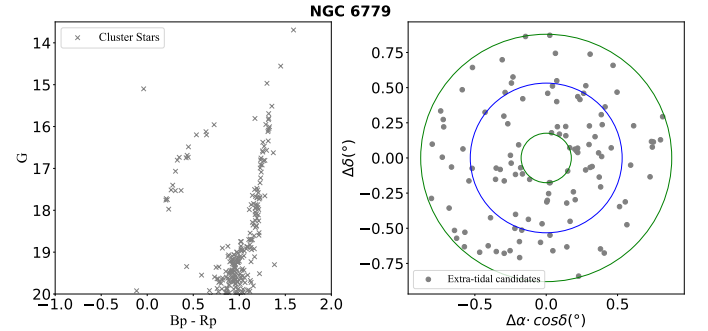


Fig. 10. Same as Fig. 6, but only CMD and spatial distribution for NGC 6779.

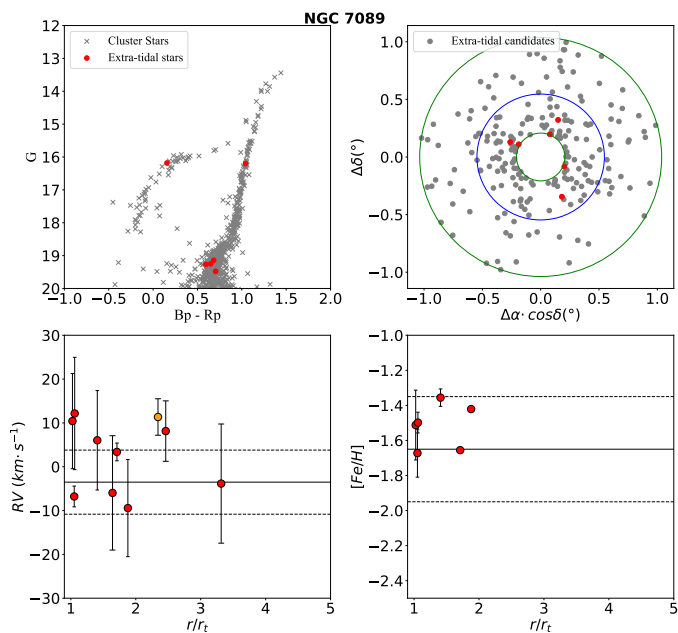


Fig. 11. Same as Fig. 6 but for NGC 7089.

and CMDs, is an efficient way to discover extra-tidal structures. The two possible density peaks at opposite directions of the inner boundary are a good indicator of a long stellar stream. Furthermore, we calculated their orbits to investigate whether some GCs are more susceptible to mass loss, thus forming stellar streams. Using GALPY, we calculated the orbits of these six GCs, beginning from 5 Gyr ago to present (Appendix A). All six GCs have high eccentricity and have traversed the Galactic disk multiple times. Notably, the pericenters of NGC 1851, NGC 1904, NGC 6341, and NGC 7089 (GCs with stellar streams) are closer to the Galactic center than the other two GCs (without stellar streams). This demonstrates that these clusters have experienced stronger tidal effects, fostering the formation of long stellar streams.

4. Summary

As one of the most ancient objects in our Galaxy, GCs are the ideal candidates to trace Galactic evolution. During their internal dynamical evolution (e.g., two-body relaxation) and their interaction with the evolving MW, GCs continuously lose stars to the field. These GC escapees are the key to fully investigating the contribution of GCs to MW halo populations. In this work we inspected GC escaped candidates under the assumption of tidal evaporation, which may account for as much as 80% of the escaped population.

If a star left its host GC a long time ago (e.g., ~ 1 Gyr), it is difficult to identify this star given its similar kinematic properties to other halo field stars. However, the distinctive chemical patterns between enriched GC stars and normal halo stars provide a possible solution. The recently found N-rich field stars are promising candidates of GC escapees. It has been suggested that the dense environment required for the production of peculiar chemical abundance, such as N enrichment, is unique to GCs. To investigate the chemodynamical links between N-rich field stars and existing GCs, we used low-resolution spectroscopic data from the LAMOST survey and astrometric data from Gaia. We created a dataset that allows the characterization of 100

N-rich field stars and existing MW GCs through their full phase-space actions and metallicity.

In this work we used dynamical action integrals to connect N-rich stars with GCs. We assumed that stars that escaped from the cluster retained their original dynamical parameters, which allowed distant stars to be considered members without being spatially adjacent to the cluster. We reported 137 possible pairs of N-rich field stars and individual GCs, of which 29 pairs were highly probable, and 16 pairs had a difference in metallicity within 0.3. Among the 29 highly probable pairs, 17 were possibly related to accretion events, such as GE, Helmi Streams, or the Sequoia galaxy. The fact that not every N-rich field star finds a GC host is probably related to the complex dynamical evolution of GCs under the ever-changing Galactic potential.

If a star left its host GC recently with tidal evaporation, it will maintain similar kinematic properties to those of its host GC. In order to identify escaped stars near clusters and provide observational samples for subsequent work (such as field stars contributed by dwarf galaxy GCs and the distribution of multiple populations), we analyzed the outer regions of six GCs that potentially relate to the GE accretion event. We identified extra-tidal candidates based on their spatial locations, PMs, and their CMD locations. We used a Gaussian mixture model (GMM) consisting of two components to estimate the mean and dispersion of the cluster PM. Then, we further confirmed the candidates by plotting the CMD of the cluster stars and corresponding isochrones based on the cluster's parameters. We found more than 1600 extra-tidal candidates in the vicinity of six clusters, including 54 extra-tidal stars, where most of the extra-tidal candidates are RGB, HB, and upper MS stars. Interestingly, we found that the density map of the extra-tidal candidates is an efficient way to discover extra-tidal structures. The two possible density peaks at opposite directions of the inner boundary is a good indicator of a long stellar stream. Additionally, spectroscopic observations are available for some candidates in four clusters. Under the assumption that GC escaped stars have the same radial velocities and metallicity as their host GCs, we confirmed that more than half ($\sim 57\%$) of the extra-tidal candidates are escaped stars beyond the tidal radius of the clusters. The high success rate bodes well for follow-up observations of our extra-tidal candidates, where the dynamical environment of GCs can be investigated.

Acknowledgements. C.X., B.T., C.L., and L.W. gratefully acknowledge support from the National Natural Science Foundation of China through grants No. 12233013, No.12073090, the Natural Science Foundation of Guangdong Province under grant No. 2022A151010732, and the China Manned Space Project Nos. CMS-CSST-2021-B03, CMS-CSST-2021-A08, etc. J.G.F.-T gratefully acknowledges the grant support provided by Proyecto Fondecyt Iniciación No. 11220340, and also from the Joint Committee ESO-Government of Chile 2021 (ORP 023/2021). L.W. thanks the support from the National Natural Science Foundation of China through grant 21BAA00619, and the one-hundred-talent project of Sun Yat-sen University, the Fundamental Research Funds for the Central Universities, Sun Yat-sen University (22hytd09).

References

- Abdurro'uf, Accetta, K., Aerts, C., et al. 2022, ApJS, 259, 35
- Abolfathi, B., Aguado, D. S., Aguilar, G., et al. 2018, ApJS, 235, 42
- Anguiano, B., De Silva, G. M., Freeman, K., et al. 2016, MNRAS, 457, 2078
- Anguiano, B., Zucker, D. B., Scholz, R. D., et al. 2015, MNRAS, 451, 1229
- Bastian, N. & Lardo, C. 2018, ARA&A, 56, 83
- Baumgardt, H. & Hilker, M. 2018, MNRAS, 478, 1520
- Baumgardt, H., Parmentier, G., Gieles, M., & Vesperini, E. 2010, MNRAS, 401, 1832
- Baumgardt, H. & Vasiliev, E. 2021, MNRAS, 505, 5957
- Belokurov, V., Erkal, D., Evans, N. W., Koposov, S. E., & Deason, A. J. 2018, MNRAS, 478, 611

- Belokurov, V., Zucker, D. B., Evans, N. W., et al. 2006, *ApJ*, 642, L137
- Binney, J. 2012, *MNRAS*, 426, 1324
- Binney, J. & Tremaine, S. 2008, *Galactic Dynamics: Second Edition*
- Bovy, J. 2015, *ApJS*, 216, 29
- Bressan, A., Marigo, P., Girardi, L., et al. 2012, *MNRAS*, 427, 127
- Buder, S., Sharma, S., Kos, J., et al. 2021, *MNRAS*, 506, 150
- Carballo-Bello, J. A., Martínez-Delgado, D., Navarrete, C., et al. 2018, *MNRAS*, 474, 683
- Carballo-Bello, J. A., Sollima, A., Martínez-Delgado, D., et al. 2014, *MNRAS*, 445, 2971
- Carlin, J. L., Liu, C., Newberg, H. J., et al. 2015, *AJ*, 150, 4
- Carretta, E., Bragaglia, A., Gratton, R. G., et al. 2010, *A&A*, 516, A55
- Cui, X.-Q., Zhao, Y.-H., Chu, Y.-Q., et al. 2012, *Research in Astronomy and Astrophysics*, 12, 1197
- de Boer, T. J. L., Gieles, M., Balbinot, E., et al. 2019, *MNRAS*, 485, 4906
- Deng, L.-C., Newberg, H. J., Liu, C., et al. 2012, *Research in Astronomy and Astrophysics*, 12, 735
- Eisenstein, D. J., Weinberg, D. H., Agol, E., et al. 2011, *AJ*, 142, 72
- Fernández-Trincado, J. G., Beers, T. C., Barbuy, B., et al. 2022, *A&A*, 663, A126
- Fernández-Trincado, J. G., Beers, T. C., & Minniti, D. 2020a, *A&A*, 644, A83
- Fernández-Trincado, J. G., Beers, T. C., Minniti, D., et al. 2020b, *ApJ*, 903, L17
- Fernández-Trincado, J. G., Beers, T. C., Minniti, D., et al. 2021a, *A&A*, 647, A64
- Fernández-Trincado, J. G., Beers, T. C., Minniti, D., et al. 2020c, *A&A*, 643, L4
- Fernández-Trincado, J. G., Beers, T. C., Placco, V. M., et al. 2019a, *ApJ*, 886, L8
- Fernández-Trincado, J. G., Beers, T. C., Queiroz, A. B. A., et al. 2021b, *ApJ*, 918, L37
- Fernández-Trincado, J. G., Beers, T. C., Tang, B., et al. 2019b, *MNRAS*, 488, 2864
- Fernández-Trincado, J. G., Chaves-Velasquez, L., Pérez-Villegas, A., et al. 2020d, *MNRAS*, 495, 4113
- Fernández-Trincado, J. G., Robin, A. C., Moreno, E., et al. 2016, *ApJ*, 833, 132
- Fernández-Trincado, J. G., Zamora, O., García-Hernández, D. A., et al. 2017, *ApJ*, 846, L2
- Forbes, D. A. & Bridges, T. 2010, *MNRAS*, 404, 1203
- Fukushige, T. & Heggie, D. C. 2000, *MNRAS*, 318, 753
- Gaia Collaboration, Brown, A. G. A., Vallenari, A., et al. 2018, *A&A*, 616, A1
- Gaia Collaboration, Brown, A. G. A., Vallenari, A., et al. 2021, *A&A*, 649, A1
- Gaia Collaboration, Prusti, T., de Bruijne, J. H. J., et al. 2016, *A&A*, 595, A1
- Gratton, R. G., Carretta, E., & Bragaglia, A. 2012, *A&A Rev.*, 20, 50
- Grillmair, C. J. 2022, *ApJ*, 929, 89
- Grillmair, C. J. & Dionatos, O. 2006, *ApJ*, 643, L17
- Hanke, M., Koch, A., Prudil, Z., Grebel, E. K., & Bastian, U. 2020, *A&A*, 637, A98
- Harris, W. E. 1996, *AJ*, 112, 1487
- Harris, W. E. 2010, *arXiv e-prints*, arXiv:1012.3224
- Helmi, A., Babusiaux, C., Koppelman, H. H., et al. 2018, *Nature*, 563, 85
- Helmi, A., White, S. D. M., de Zeeuw, P. T., & Zhao, H. 1999, *Nature*, 402, 53
- Huang, Y., Liu, X. W., Yuan, H. B., et al. 2015, *MNRAS*, 449, 162
- Huang, Y., Liu, X. W., Yuan, H. B., et al. 2016, *MNRAS*, 463, 2623
- Ibata, R., Malhan, K., Martin, N., et al. 2021, *ApJ*, 914, 123
- Ibata, R. A., Bellazzini, M., Malhan, K., Martin, N., & Bianchini, P. 2019, *Nature Astronomy*, 3, 667
- Ibata, R. A., Gilmore, G., & Irwin, M. J. 1994, *Nature*, 370, 194
- Johnson, C. I. & Pilachowski, C. A. 2012, *ApJ*, 754, L38
- Jordi, K. & Grebel, E. K. 2010, *A&A*, 522, A71
- Koch, A., Grebel, E. K., & Martell, S. L. 2019, *A&A*, 625, A75
- Kundu, R., Fernández-Trincado, J. G., Minniti, D., et al. 2019, *MNRAS*, 489, 4565
- Kundu, R., Navarrete, C., Fernández-Trincado, J. G., et al. 2021, *A&A*, 645, A116
- Kundu, R., Navarrete, C., Sbordone, L., et al. 2022, *A&A*, 665, A8
- Küpper, A. H. W., Kroupa, P., Baumgardt, H., & Heggie, D. C. 2010, *MNRAS*, 407, 2241
- Kuzma, P. B., Da Costa, G. S., & Mackey, A. D. 2018, *MNRAS*, 473, 2881
- Kuzma, P. B., Da Costa, G. S., Mackey, A. D., & Roderick, T. A. 2016, *MNRAS*, 461, 3639
- Li, C., Tang, B., Milone, A. P., et al. 2021, *ApJ*, 906, 133
- Limberg, G., Souza, S. O., Pérez-Villegas, A., et al. 2022, *ApJ*, 935, 109
- Lind, K., Katosov, S. E., Battistini, C., et al. 2015, *A&A*, 575, L12
- Majewski, S. R., Schiavon, R. P., Frinchaboy, P. M., et al. 2017, *AJ*, 154, 94
- Malhan, K., Ibata, R. A., & Martin, N. F. 2018, *MNRAS*, 481, 3442
- Malhan, K., Ibata, R. A., Sharma, S., et al. 2022, *ApJ*, 926, 107
- Marigo, P., Girardi, L., Bressan, A., et al. 2017, *ApJ*, 835, 77
- Marino, A. F., Milone, A. P., Yong, D., et al. 2014, *MNRAS*, 442, 3044
- Martell, S. L. & Grebel, E. K. 2010, *A&A*, 519, A14
- Martell, S. L., Shetrone, M. D., Lucatello, S., et al. 2016, *ApJ*, 825, 146
- Martell, S. L., Smolinski, J. P., Beers, T. C., & Grebel, E. K. 2011, *A&A*, 534, A136
- Massari, D., Koppelman, H. H., & Helmi, A. 2019, *A&A*, 630, L4
- Mateu, C. 2023, *MNRAS*, 520, 5225
- Mészáros, S., Martell, S. L., Shetrone, M., et al. 2015, *AJ*, 149, 153
- Milone, A. P., Marino, A. F., Piotto, G., et al. 2015a, *MNRAS*, 447, 927
- Milone, A. P., Marino, A. F., Piotto, G., et al. 2015b, *ApJ*, 808, 51
- Myeong, G. C., Vasiliev, E., Iorio, G., Evans, N. W., & Belokurov, V. 2019, *MNRAS*, 488, 1235
- Odenkirchen, M., Grebel, E. K., Rockosi, C. M., et al. 2001, *ApJ*, 548, L165
- Olszewski, E. W., Saha, A., Knezek, P., et al. 2009, *AJ*, 138, 1570
- Pedregosa, F., Varoquaux, G., Gramfort, A., et al. 2011, *Journal of Machine Learning Research*, 12, 2825
- Piatti, A. E. & Carballo-Bello, J. A. 2019, *MNRAS*, 485, 1029
- Piotto, G., Milone, A. P., Anderson, J., et al. 2012, *ApJ*, 760, 39
- Randich, S., Gilmore, G., Magrini, L., et al. 2022, *A&A*, 666, A121
- Sariya, D. P. & Yadav, R. K. S. 2015, *A&A*, 584, A59
- Savino, A. & Posti, L. 2019, *A&A*, 624, L9
- Schiavon, R. P., Zamora, O., Carrera, R., et al. 2017, *MNRAS*, 465, 501
- Schönrich, R., Binney, J., & Dehnen, W. 2010, *MNRAS*, 403, 1829
- Shipp, N., Drlica-Wagner, A., Balbinot, E., et al. 2018, *ApJ*, 862, 114
- Snedden, C., Kraft, R. P., Guhathakurta, P., Peterson, R. C., & Fulbright, J. P. 2004, *AJ*, 127, 2162
- Sollima, A. 2020, *MNRAS*, 495, 2222
- Sparke, L. S. & Gallagher, John S., I. 2000, *Galaxies in the universe : an introduction*
- Steinmetz, M., Matijevic, G., Enke, H., et al. 2020, *VizieR Online Data Catalog*, III/283
- Tang, B., Cohen, R. E., Geisler, D., et al. 2017, *MNRAS*, 465, 19
- Tang, B., Fernández-Trincado, J. G., Geisler, D., et al. 2018, *ApJ*, 855, 38
- Tang, B., Fernández-Trincado, J. G., Liu, C., et al. 2020, *ApJ*, 891, 28
- Tang, B., Liu, C., Fernández-Trincado, J. G., et al. 2019, *ApJ*, 871, 58
- Tang, B., Wang, Y., Huang, R., et al. 2021, *ApJ*, 908, 220
- Testa, V., Zaggia, S. R., Andreon, S., et al. 2000, *A&A*, 356, 127
- Thomas, G. F., Jensen, J., McConnachie, A., et al. 2020, *ApJ*, 902, 89
- Valcarce, A. A. R., Catelan, M., & Sweigart, A. V. 2012, *A&A*, 547, A5
- Vasiliev, E. & Baumgardt, H. 2021, *MNRAS*, 505, 5978
- Wan, Z., Lewis, G. F., Li, T. S., et al. 2020, *Nature*, 583, 768
- Wan, Z., Oliver, W. H., Baumgardt, H., et al. 2021, *MNRAS*, 502, 4513
- Weatherford, N. C., Kiroğlu, F., Fragione, G., et al. 2023, *ApJ*, 946, 104
- Yanny, B., Rockosi, C., Newberg, H. J., et al. 2009, *AJ*, 137, 4377
- Yong, D., Roederer, I. U., Grundahl, F., et al. 2014, *MNRAS*, 441, 3396
- Yu, J., Tang, B., Fernández-Trincado, J. G., et al. 2021, *ApJ*, 913, 23
- Zhao, G., Zhao, Y.-H., Chu, Y.-Q., Jing, Y.-P., & Deng, L.-C. 2012, *Research in Astronomy and Astrophysics*, 12, 723
- Zhou, Y., Li, X., Huang, Y., & Zhang, H. 2023, *ApJ*, 946, 73

Appendix A: Orbits of 6 GCs in Sec 3.2

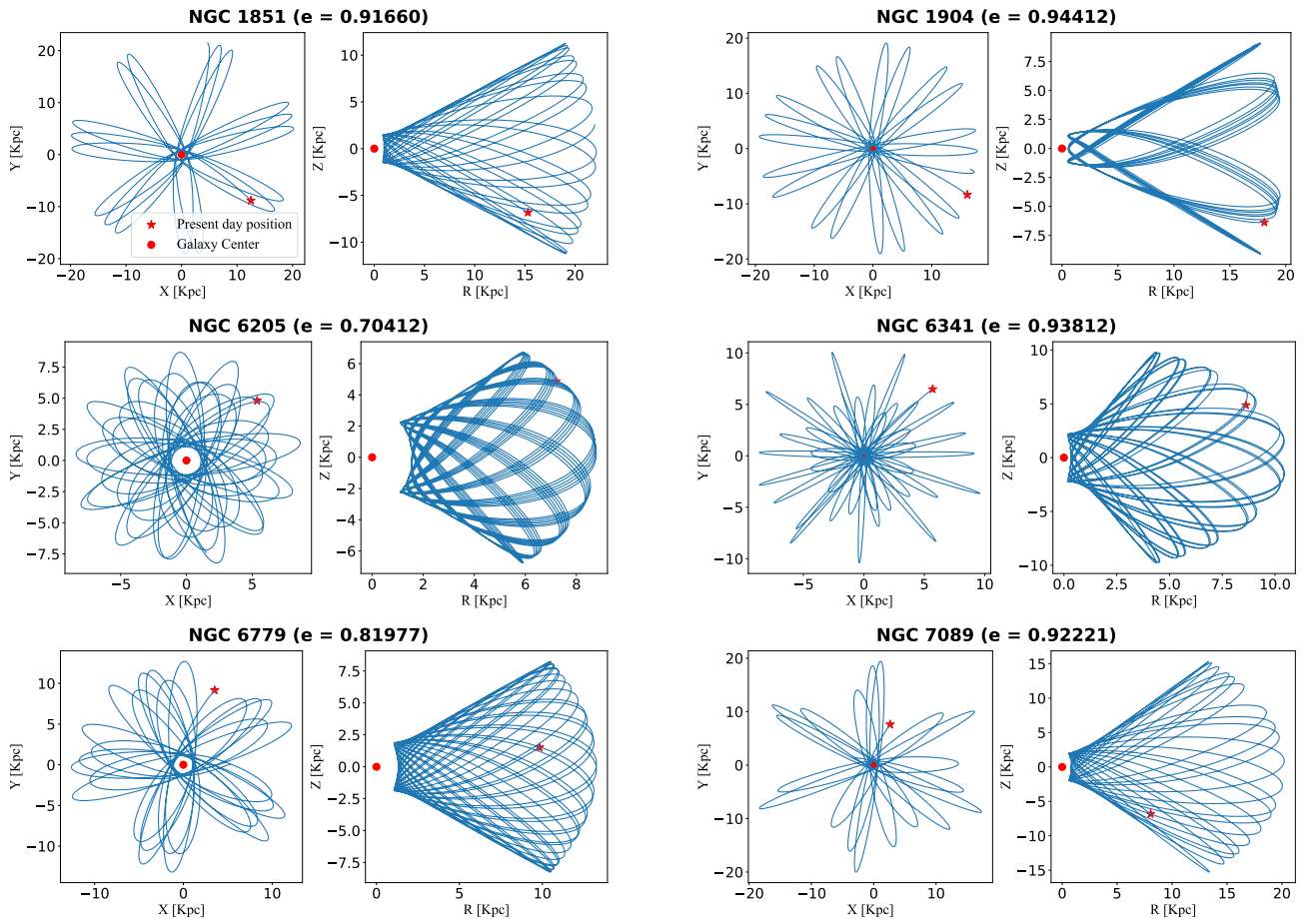


Fig. A.1. Orbits of NGC 1851, NGC 1904, NGC 6205, NGC 6341, NGC 6779 and NGC 7089.